FRACTURE AND DAMAGE IN BOTH NANOPHASE AND CERAMICS : ON THE MORPHOLOGY OF FRACTURE SURFACES.

L. Ponson [1,2], D. Bonamy[1], H. Auradou[2], E. Bouchaud[1], C. Guillot[1], E. Fairbairn[3] & J.-P. Hulin[2]
[1] Groupe Fracture, Service de Physique & Chimie des Surfaces et Interfaces, DSM/DRECAM CEA Saclay, F-91191 Gif sur Yvette, France
[2] Laboratoire Fluides, Automatiques & Systèmes Thermiques, Université Paris XI, 91405 Orsay, France
[3] COPPE/The post-Graduate Engineering Institute, Universitade Federal do Rio de Janeiro, C.P. 68506, CEP 21945-970-Rio de Janeiro-RJ-Brazil

ABSTRACT

The present study was designed to determine the role of the microstructure length-scales in fracture mechanisms in heterogeneous media. Therefore, materials of various grains sizes, *i.e.* nanophase TiO_2 (grains size around 300 nanometers), zirconolite ceramics (grains size around 10 micrometers) and glass ceramics (grain size around 100 micrometers) were fractured in both dynamic and sub-critical stress corrosion regime. Combinations of Atomic Force Microscopy and stylus profilometry were used to measure the topography of post-mortem fracture surfaces. In glass ceramics, these surfaces are found to be self-affine, with a roughness exponent $\zeta \sim 0.5$, significantly smaller than $\zeta = 0.8$ as commonly observed for homogeneous glass. In nanophase TiO_2, ζ was found to be even smaller, close to zero. Development of roughness during crack propagation was also investigated. Influence of both grain size and cohesion strength between grains on self-affine properties of post-mortem fracture surfaces will finally be discussed.

1 INTRODUCTION

Trivially enough, the fracture surface of heterogeneous materials is rough. As a matter of fact, this roughness conveys the complex interactions between a propagating crack front and the material microstructure. Fractography analysis revealed that the topography of these surfaces exhibit scale invariant character, - referred to as self-affinity -, extending over a wide range of length-scales [1-4]. The roughness exponent ζ was found close to 0.8 in many materials (glass, wood, ceramics, concrete, ductile metals, granite…) and for many different fracture modes (dynamic fracture, fatigue, stress corrosion). It was then conjectured to be *universal*, which gives rise to an important theoretical effort [5-8]. All these models failed to reproduce the exponent $\zeta \sim 0.8$ as observed experimentally.

More recently, experimental study of fracture surface roughness on sandstone [9] reports another roughness $\zeta \sim 0.5$ significantly smaller than the previous one. The intergranular nature of fracture was suggested to explain the differences between the values of roughness exponents.

The present study is designed to address this question. The experimental setup is described in section 2. Materials of various microstructure length-scales, *i.e.* nanophase TiO_2, zirconolite ceramics and glass ceramics are broken. A wide range of crack growth velocities, ranging from 10^{-7}m.s^{-1} (stress corrosion regime) to significant fraction of the sound speed (dynamic regime) is also investigated. Fractography analysis was performed using combinations of Atomic Force Microscopy and stylus profilometry and the self affine properties of the fracture surfaces were deduced (section 3). In glass ceramics, these surfaces are found to be self-affine, with a roughness exponent $\zeta \sim 0.5$. In nanophase TiO_2, ζ was found to be even smaller, close to zero. This is finally discussed.

2 EXPERIMENTAL SETUP

Depending on the materials and on the investigated crack velocities, different fracture geometries were used:

1. Both dynamic and sub-critical stress corrosion fractures in nanophase TiO_2 and zirconolite ceramics were generated in DCDC (double cleavage drilled compression) parallepipedic ($2.5\times2.5\times20$ mm^3) samples [10,11]. The experimental setup is shown in Fig. 1. In the center of two parallel $2.5\times20mm^2$ surfaces and perpendicular to them, a cylindrical hole (radius of 0.4 mm) is drilled. The sample is placed in a compressive machine that applies an external stress on the two opposite 2.5×2.5 mm^2 surfaces. The applied load, - measured through a stress gauge -, is gradually increased. Once two cracks are initiated (symmetrically to the hole axis), the jaw displacement is stopped and the force is kept constant. First, the crack propagates very quickly (Dynamic fracture regime). As the crack length increases, K_I decreases. Above a critical crack length c_* (around 3 mm), K_I falls below the toughness K_{Ic}. The crack then continues to propagate under stress corrosion, at much smaller speed (measured around 10^{-7} $m.s^{-1}$).

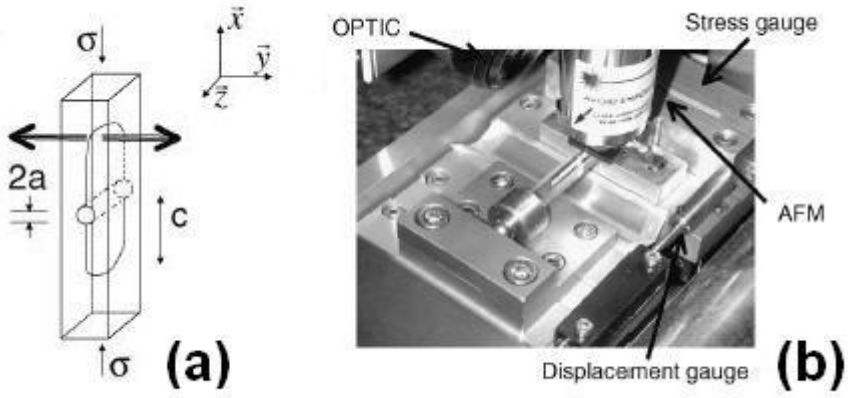

Fig. 1. Experimental setup: (a) sketch of the DCDC geometry; (b) picture of the experiment.

2. Dynamic fractures in glass ceramics were obtained using modified Brazilian test geometry [12]. The experimental setup is shown in Fig. 2. Cylindrical tubes of 70 mm external diameter, 30 mm internal diameter and 20 mm thickness were placed in a compressive machine. The sample is placed so that its symmetry axis is perpendicular to the applied force. The applied load is gradually increased up to fracture initiation. The crack then propagates dynamically up to the complete failure of the specimen.

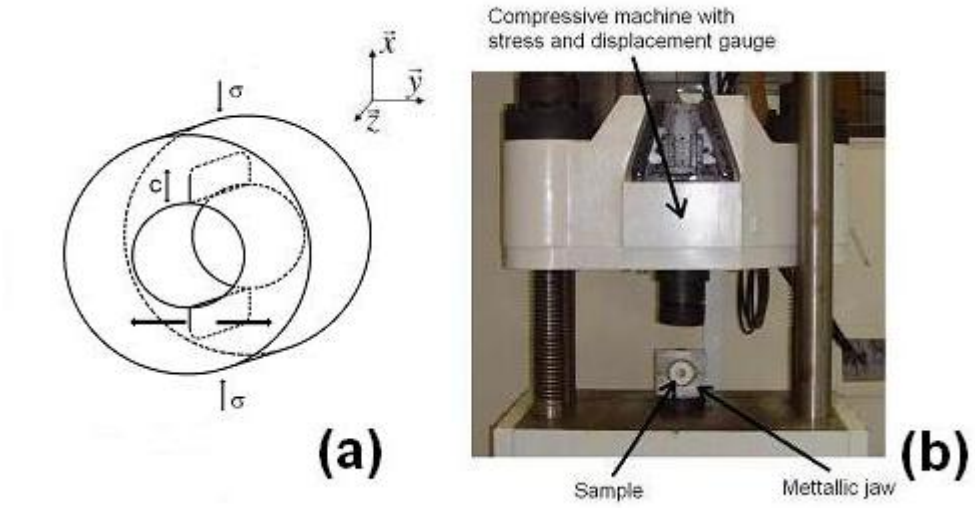

Fig. 2. Experimental setup: (a) sketch of the modified Brazilian test geometry; (b) picture of the experiment.

3. Stable quasi-static fracture in glass ceramics were propagated in modified TDCB geometry [13]. The experimental setup is shown in Fig. 3. A trapezoidal sample of length 70 mm, of larger width 40 mm, of smaller width 22 mm and of thickness 25 mm is cut. A 20 mm seed crack was introduced parallel to the length from the smaller side of the specimen. This sample was placed between two jaws in a tensile machine. The traction is then increased at constant velocities. The crack then propagates quasi-statically at a constant velocity controlled by the jaws velocity. In this specific geometry, the crack velocity was also measured via potential drop method.

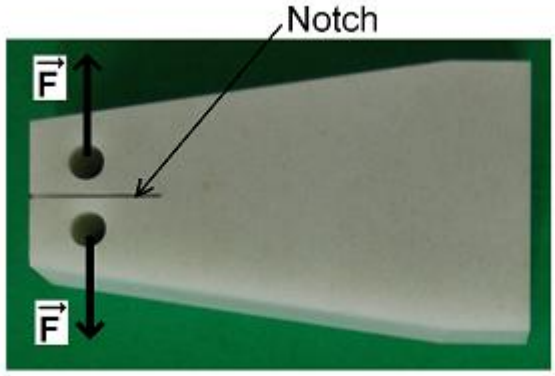

Fig. 3. Experimental setup: picture of the modified TDCB geometry.

For all these tests, variation of the stress intensity factors with respect to both the crack length and applied solicitation was computed through Finite Elements (FE) simulations.

Topography of the fracture surfaces is then measured *post-mortem*. Atomic Force Microscopy is used for nanophase TiO_2. Lateral resolution and Vertical resolution are estimated around 5 nanometers and 1 Angstrom respectively. The main drawback of this device resides in the maximum scan size, limited to 35 micrometer. Topography of ceramics was measured through Stylus profilometry with a lateral resolution of 1 micrometer and a vertical resolution of 10 nanometers.

3 EXPERIMENTAL RESULTS

Figure 4a and b presents the topography of post-mortem fracture surfaces in glass ceramics and nanophase TiO_2 respectively. Fracture surfaces in heterogeneous materials have been extensively investigated over the last 20 years [1-4]. For a wide range of materials (glass, wood, ceramics, ductile metals…), they were found to exhibit self-affine properties. This leads us to look at the statistical analysis of the fracture surface morphology in these two sintered materials. Detrended Fluctuation analysis (DFA) was used to exhibit the self-affine properties of our surfaces. In short, DFA consists in dividing each scanning line of the images into nonoverlapping boxes of size Δr. The best linear trend is defined in each box and subtracted to each box. The standard deviation of this redressed profile within the box is then calculated and averaged over all the boxes of the same size Δr and all lines. For a self-affine profile of roughness exponent ζ one gets:

$$\sigma^2 \propto \Delta r^{2\zeta}$$

where σ is the averaged detrended standard deviation on box of size Δr.

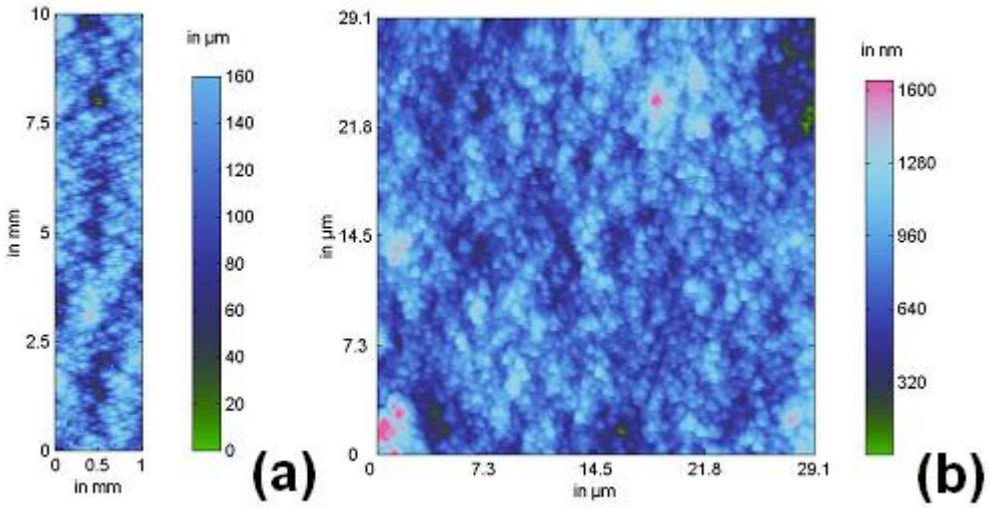

Fig. 4. Fracture surface topography: (a) in glass ceramics measured by stylus profilometry; (b) in nanophase TiO_2 measured by atomic force microscopy. The both are fractured in dynamic regime.

Figure 5a and b presents the DFA curves obtained for glass ceramics and nanophase TiO_2 respectively. For glass ceramics, a self-affine regime ranging from the grain size (around 100 micrometers) to several millimeters is evidenced. The roughness exponent ζ is found to be $\zeta \sim 0.5$. The value of this roughness exponent was confirmed using others estimators (wavelet transforms,

zmax methods and typical height method). Such roughness exponent was also observed for sandstone fracture surfaces [9]. However, this exponent is significantly smaller than the roughness exponent ζ~0.8 as commonly observed over a wide range of materials (glass, wood, ceramics, ductile metals…) [1-4]. Understanding the role of the ceramic porosity is currently under progress. For nanophase TiO_2, our DFA curves are more compatible with logarithmic roughening than self-affine ones. This is not commonly observed, but predicted theoretically [6]. This may be attributed to low cohesive strength between grains. This is currently explored.

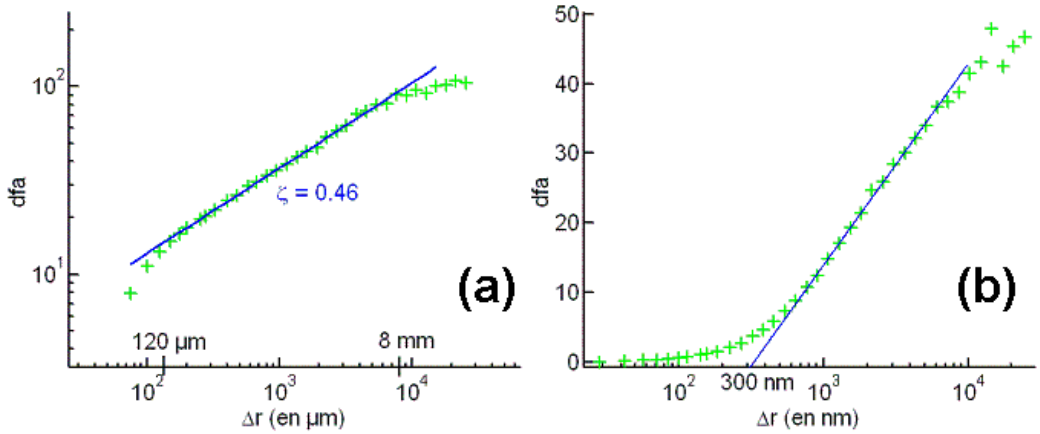

Fig.5. DFA curves obtained: (a) in glass ceramics; (b) in nanophase TiO_2.

4 CONCLUDING REMARKS

We have carried out investigation of the self-affine properties of fracture surfaces in sintered materials with various grains sizes, ranging from 300 nanometers (nanophase TiO_2) to 100 micrometers (glass ceramics). Different roughness exponents ζ were found: $\zeta \sim 0.5$ in glass ceramics while fracture surfaces in nanophase TiO_2 are more compatible with a logarithmic roughness. Possible origin of the values of these two exponents is currently explored. Development of roughness during crack propagation is also currently investigated.

5 REFERENCES

[1] B. B. Mandelbrot, D. E. Passoja, A. J. Paullay, Fractal character of fracture surfaces of metals. *Nature* **308**. 721-722 (1984).
[2] E. Bouchaud, Scaling properties of cracks. *J. Phys.-Condens. Matt*. **9**. 4319-4344 (1997) (and references therein).
[3] J. Schmittbuhl, F. Schmitt, C. Scholz, Scaling invariance of crack surfaces. *J. Geophys. res.* **100**. 5953-5973 (1995).
[4] K. J. Maloy, A. Hansen, E. L. Hinrichsen, S. Roux, Experimental measurements of the roughness of brittle cracks. *Phys. Rev. Lett.* **68**. 213-215 (1992).
[5] D. Ertas, M. Kardar, Dynamic roughening of directed lines. *Phys. Rev. Lett.* **69**. 929 (1992).
[6] S. Ramanathan, D. Ertas, D. S. Fisher, Quasistatic crack propagation in heterogeneous media. *Phys. Rev. Lett.* **79**. 873 (1997).
[7] S. Ramanathan, D. S. Fisher, Dynamics and instabilities of planar tensile cracks in heterogeneous media. *Phys. Rev. Lett.* **79**. 877 (1997).

[8] E. Bouchaud, J. P. Bouchaud, D. S. Fisher, S. Ramanathan, J. R. Rice, Can crack front waves explain the roughness of cracks? *J. Mech. Phys. Solids* **50**. 1703-1725 (2002).
[9] J. M. Boffa, C. Allain, J. P. Hulin, Experimental analysis of fracture rugosity in granular and compact rocks. Eur. Phys. J. **2**. 281-289 (1998).
[10] C. Janssen, Specimen for fracture mechanics studies on glass in *Proc. 10th Int. Cong. on glass, Tokyo*. 10.23-10.30 (1974).
[11] M. Y. He, M. R. Turner, A. G. Evans, Analysis of the double cleavage drilled compression specimen for interface fracture energy measurements over range of mode mixities. *Act. Metall. Mat*. **43**. 3453-3458 (1995).
[12] F. L. Carneiro, A. Barcellos, Résistance à la traction des Bétons. *Int. Assoc. Test. Lab. Matter. Struct.* **13**. 98-125 (1949).
[13] S. Morel, J. Schmittbuhl, J. Lopez, G. Valentin, Anomalous roughening of wood fracture surfaces. *Phys. Rev. E.* **58**. 6999-7005 (1998).